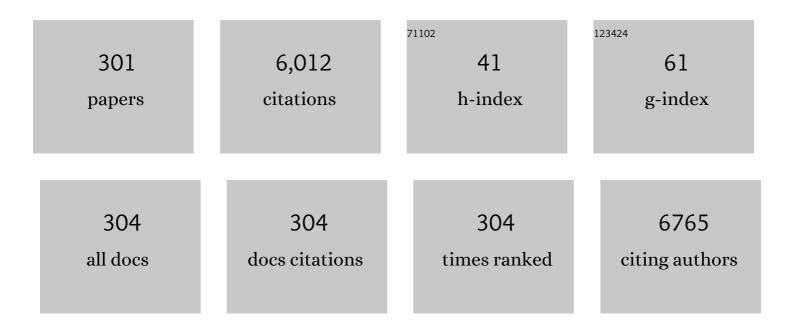
List of Publications by Year in descending order

Source: https://exaly.com/author-pdf/7335146/publications.pdf Version: 2024-02-01



#	Article	IF	CITATIONS
1	Carbon monoxide (CO) optical gas sensor based on ZnO thin films. Sensors and Actuators B: Chemical, 2017, 250, 679-685.	7.8	156
2	NiO nanoparticle-based urea biosensor. Biosensors and Bioelectronics, 2013, 41, 110-115.	10.1	149
3	SnO2 thin film sensor with enhanced response for NO2 gas at lower temperatures. Sensors and Actuators B: Chemical, 2011, 156, 743-752.	7.8	148
4	Flower-like ZnO nanostructure based electrochemical DNA biosensor for bacterial meningitis detection. Biosensors and Bioelectronics, 2014, 59, 200-207.	10.1	131
5	Metal oxide catalyst assisted SnO2 thin film based SO2 gas sensor. Sensors and Actuators B: Chemical, 2016, 224, 282-289.	7.8	124
6	A comparative study of RGO-SnO2 and MWCNT-SnO2 nanocomposites based SO2 gas sensors. Sensors and Actuators B: Chemical, 2017, 248, 980-986.	7.8	110
7	Room temperature trace level detection of NO2 gas using SnO2 modified carbon nanotubes based sensor. Journal of Materials Chemistry, 2012, 22, 23608.	6.7	106
8	Metal clusters activated SnO2 thin film for low level detection of NH3 gas. Sensors and Actuators B: Chemical, 2014, 194, 410-418.	7.8	103
9	Fabrication and characterization of ZnO-TiO2-PANI (ZTP) micro/nanoballs for the detection of flammable and toxic gases. Journal of Hazardous Materials, 2019, 370, 126-137.	12.4	96
10	Highly sensitive and selective uric acid biosensor based on RF sputtered NiO thin film. Biosensors and Bioelectronics, 2011, 30, 333-336.	10.1	93
11	Enhanced response characteristics of SnO2 thin film based NO2 gas sensor integrated with nanoscaled metal oxide clusters. Sensors and Actuators B: Chemical, 2013, 181, 735-742.	7.8	92
12	CuO thin film based uric acid biosensor with enhanced response characteristics. Biosensors and Bioelectronics, 2012, 38, 11-18.	10.1	85
13	ZnO/ST-Quartz SAW resonator: An efficient NO2 gas sensor. Sensors and Actuators B: Chemical, 2017, 252, 840-845.	7.8	81
14	Nitrogen-doped zinc oxide thin films biosensor for determination of uric acid. Analyst, The, 2013, 138, 4353.	3.5	79
15	Synthesis of CdS nanoparticle by sol-gel method as low temperature NO2 sensor. Materials Chemistry and Physics, 2020, 239, 121975.	4.0	78
16	WO3 nanoclusters–SnO2 film gas sensor heterostructure with enhanced response for NO2. Sensors and Actuators B: Chemical, 2013, 176, 675-684.	7.8	73
17	Development of a microfluidic electrochemical biosensor: Prospect for point-of-care cholesterol monitoring. Sensors and Actuators B: Chemical, 2018, 261, 460-466.	7.8	73
18	Zinc oxide–multiwalled carbon nanotubes hybrid nanocomposite based urea biosensor. Journal of Materials Chemistry B, 2013, 1, 6392.	5.8	71

#	Article	IF	CITATIONS
19	ZnO–CuO composite matrix based reagentless biosensor for detection of total cholesterol. Biosensors and Bioelectronics, 2015, 67, 263-271.	10.1	65
20	Highly sensitive and non-invasive electrochemical immunosensor for salivary cortisol detection. Sensors and Actuators B: Chemical, 2019, 293, 281-288.	7.8	63
21	Ferroelectric photovoltaic properties of Ce and Mn codoped BiFeO3 thin film. Journal of Applied Physics, 2014, 115, .	2.5	58
22	A low temperature operated NO2 gas sensor based on TeO2/SnO2 p–n heterointerface. Sensors and Actuators B: Chemical, 2013, 176, 875-883.	7.8	56
23	Optical properties of WO3 thin films using surface plasmon resonance technique. Journal of Applied Physics, 2014, 115, .	2.5	56
24	Room temperature detection of NO2 gas using optical sensor based on surface plasmon resonance technique. Sensors and Actuators B: Chemical, 2015, 216, 497-503.	7.8	56
25	Optimization of excess Bi doping to enhance ferroic orders of spin casted BiFeO3 thin film. Journal of Applied Physics, 2014, 115, .	2.5	55
26	Enhancement in NH3 sensing performance of ZnO thin-film via gamma-irradiation. Journal of Alloys and Compounds, 2020, 830, 154641.	5.5	55
27	Low temperature operating SnO2 thin film sensor loaded with WO3 micro-discs with enhanced response for NO2 gas. Sensors and Actuators B: Chemical, 2012, 161, 1114-1118.	7.8	54
28	Enhanced microwave absorption and suppressed reflection of polypyrrole-cobalt ferrite-graphene nanocomposite in X-band. Journal of Alloys and Compounds, 2019, 797, 1190-1197.	5.5	54
29	Complex dielectric constant of various biomolecules as a function of wavelength using surface plasmon resonance. Journal of Applied Physics, 2014, 116, .	2.5	53
30	Enhanced CO gas sensing properties of Cu doped SnO <sub>2</sub> nanostructures prepared by a facile wet chemical method. Physical Chemistry Chemical Physics, 2016, 18, 18846-18854.	2.8	52
31	Fabrication of an efficient GLAD-assisted p-NiO nanorod/n-ZnO thin film heterojunction UV photodiode. Journal of Materials Chemistry C, 2014, 2, 2387.	5.5	51
32	Electromagnetic interference shielding performance of lightweight NiFe2O4/rGO nanocomposite in X- band frequency range. Ceramics International, 2020, 46, 15473-15481.	4.8	50
33	Influence of hole mobility on the response characteristics of p-type nickel oxide thin film based glucose biosensor. Analytica Chimica Acta, 2012, 726, 93-101.	5.4	48
34	Highly sensitive Love wave acoustic biosensor for uric acid. Sensors and Actuators B: Chemical, 2018, 261, 169-177.	7.8	48
35	Glad assisted synthesis of NiO nanorods for realization of enzymatic reagentless urea biosensor. Biosensors and Bioelectronics, 2014, 52, 196-201.	10.1	46
36	Custom designed metal anchored SnO2 sensor forÂH2 detection. International Journal of Hydrogen Energy, 2017, 42, 4597-4609.	7.1	46

#	Article	IF	CITATIONS
37	Improved electromagnetic shielding behaviour of graphene encapsulated polypyrrole-graphene nanocomposite in X-band. Composites Science and Technology, 2020, 192, 108113.	7.8	46
38	Temperature stability ofc-axis oriented LiNbO3/SiO2/Si thin film layered structures. Journal Physics D: Applied Physics, 2001, 34, 2267-2273.	2.8	45
39	Ce-doped bismuth ferrite thin films with improved electrical and functional properties. Journal of Materials Science, 2014, 49, 5355-5364.	3.7	45
40	SnO2 thin film sensor having NiO catalyst for detection of SO2 gas with improved response characteristics. Sensors and Actuators B: Chemical, 2017, 248, 998-1005.	7.8	44
41	Zn doping induced conductivity transformation in NiO films for realization of p-n homo junction diode. Journal of Applied Physics, 2017, 121, .	2.5	42
42	Investigation of structural, optical, dielectric and magnetic studies of Mn substituted BiFeO3 multiferroics. Ceramics International, 2017, 43, 13750-13758.	4.8	40
43	Label-free amperometric biosensor for Escherichia coli O157:H7 detection. Applied Surface Science, 2019, 495, 143548.	6.1	40
44	Realization of an efficient cholesterol biosensor using ZnO nanostructured thin film. Analyst, The, 2012, 137, 5854.	3.5	39
45	Enhanced ferroelectric photovoltaic response of BiFeO3/BaTiO3 multilayered structure. Journal of Applied Physics, 2015, 118, .	2.5	38
46	Molybdenum Disulfide-Wrapped Carbon Nanotube-Reduced Graphene Oxide (CNT/MoS <sub>2</sub> -rGO) Nanohybrids for Excellent and Fast Removal of Electromagnetic Interference Pollution. ACS Applied Materials & Interfaces, 2020, 12, 40828-40837.	8.0	38
47	Raman spectroscopy of nanocrystalline Mn-doped BiFeO <sub>3</sub> thin films. Journal of Experimental Nanoscience, 2013, 8, 261-266.	2.4	37
48	Trap assisted space charge conduction in p-NiO/n-ZnO heterojunction diode. Materials Research Bulletin, 2015, 66, 123-131.	5.2	37
49	Performance of magnetoelectric PZT/Ni multiferroic system for energy harvesting application. Smart Materials and Structures, 2017, 26, 035002.	3.5	37
50	Distinct detection of liquor ammonia by ZnO/SAW sensor: Study of complete sensing mechanism. Sensors and Actuators B: Chemical, 2017, 238, 83-90.	7.8	37
51	CoFe <sub>2</sub> O <sub>4</sub> nanoparticles decorated MoS <sub>2</sub> -reduced graphene oxide nanocomposite for improved microwave absorption and shielding performance. RSC Advances, 2019, 9, 21881-21892.	3.6	37
52	Influence of samarium doping on magnetic and structural properties of M type Ba–Co hexaferrite. Ceramics International, 2016, 42, 8413-8418.	4.8	36
53	Effect of non-magnetic Al3+ doping on structural, optical, electrical, dielectric and magnetic properties of BiFeO3 ceramics. Ceramics International, 2018, 44, 4711-4718.	4.8	36
54	P-N Junction of NiO Thin Film for Photonic Devices. IEEE Electron Device Letters, 2013, 34, 81-83.	3.9	35

#	Article	IF	CITATIONS
55	Structural and magnetic properties of N doped ZnO thin films. Journal of Applied Physics, 2012, 111, .	2.5	34
56	Effect of metal oxide sensing layers on the distinct detection of ammonia using surface acoustic wave (SAW) sensors. Sensors and Actuators B: Chemical, 2013, 187, 563-573.	7.8	34
57	Multiferroic properties of BiFeO3/BaTiO3 multilayered thin films. Physica B: Condensed Matter, 2014, 448, 125-127.	2.7	34
58	Raman scattering and photoluminescence investigations of N doped ZnO thin films: Local vibrational modes and induced ferromagnetism. Journal of Applied Physics, 2016, 120, .	2.5	34
59	High performance UV photodetector based on MoS2 layers grown by pulsed laser deposition technique. Journal of Alloys and Compounds, 2020, 835, 155222.	5.5	34
60	Sol–gel derived Ag-doped ZnO thin film for UV photodetector with enhanced response. Journal of Materials Science, 2013, 48, 7994-8002.	3.7	33
61	Detection of Neisseria meningitidis using surface plasmon resonance based DNA biosensor. Biosensors and Bioelectronics, 2016, 78, 106-110.	10.1	33
62	EMI shielding of MWCNT/ABS nanocomposites in contrast to graphite/ABS composites and MWCNT/PS nanocomposites. RSC Advances, 2016, 6, 45049-45058.	3.6	32
63	Long Range Surface Plasmons assisted highly sensitive and room temperature operated NO2 gas sensor. Sensors and Actuators B: Chemical, 2020, 311, 127897.	7.8	31
64	Growth and characterization of c-axis oriented LiNbO3 film on a transparent conducting Al:ZnO inter-layer on Si. Journal of Materials Research, 2004, 19, 2235-2239.	2.6	30
65	Purely hopping conduction in c-axis oriented LiNbO3 thin films. Journal of Applied Physics, 2009, 105, .	2.5	30
66	Novel scheme to improve SnO2/SAW sensor performance for NO2 gas by detuning the sensor oscillator frequency. Sensors and Actuators B: Chemical, 2015, 220, 154-161.	7.8	30
67	Realization of a label-free electrochemical immunosensor for detection of low density lipoprotein using NiO thin film. Biosensors and Bioelectronics, 2016, 80, 294-299.	10.1	30
68	Cytogenetic and hematological alterations induced by acute oral exposure of imidacloprid in female mice. Drug and Chemical Toxicology, 2016, 39, 59-65.	2.3	30
69	Photovoltaic effect in BiFeO3/BaTiO3 multilayer structure fabricated by chemical solution deposition technique. Journal of Physics and Chemistry of Solids, 2016, 93, 63-67.	4.0	29
70	Nanostructured NiO-based reagentless biosensor for total cholesterol and low density lipoprotein detection. Analytical and Bioanalytical Chemistry, 2017, 409, 1995-2005.	3.7	29
71	A novel low-powered uric acid biosensor based on arrayed p-n junction heterostructures of ZnO thin film and CuO microclusters. Sensors and Actuators B: Chemical, 2017, 253, 566-575.	7.8	29
72	Fabrication of surface acoustic wave based wireless NO 2 gas sensor. Surface and Coatings Technology, 2018, 343, 89-92.	4.8	29

#	Article	IF	CITATIONS
73	Refractive Index Sensor Using Long-Range Surface Plasmon Resonance with Prism Coupler. Plasmonics, 2019, 14, 375-381.	3.4	29
74	Effect of processing parameters for electrocatalytic properties of SnO2 thin film matrix for uric acid biosensor. Analyst, The, 2014, 139, 837.	3.5	28
75	Growth of highly porous ZnO nanostructures for carbon monoxide gas sensing. Surface and Coatings Technology, 2018, 343, 49-56.	4.8	28
76	Multifunctional CuO Nanosheets for High-Performance Supercapacitor Electrodes with Enhanced Photocatalytic Activity. Journal of Inorganic and Organometallic Polymers and Materials, 2019, 29, 1067-1075.	3.7	28
77	Piezoresponse force microscopy and vibrating sample magnetometer study of single phased Mn induced multiferroic BiFeO3 thin film. Journal of Applied Physics, 2012, 111, .	2.5	27
78	Inducing electrocatalytic functionality in ZnO thin film by N doping to realize a third generation uric acid biosensor. Biosensors and Bioelectronics, 2014, 55, 57-65.	10.1	26
79	A highly efficient urea detection using flower-like zinc oxide nanostructures. Materials Science and Engineering C, 2015, 57, 38-48.	7.3	26
80	Origin and role of elasticity in the enhanced DMMP detection by ZnO/SAW sensor. Sensors and Actuators B: Chemical, 2015, 207, 375-382.	7.8	26
81	Surface plasmon resonance study on the optical sensing properties of tin oxide (SnO2) films to NH3 gas. Journal of Applied Physics, 2016, 119, .	2.5	26
82	Sensitive optical biosensor based on surface plasmon resonance using ZnO/Au bilayered structure. Optik, 2016, 127, 7642-7647.	2.9	26
83	Pyrene appended bis-triazolylated 1,4-dihydropyridine as a selective fluorogenic sensor for Cu2+. Dyes and Pigments, 2019, 161, 162-171.	3.7	26
84	Temperature coefficient of elastic constants of SiO2over-layer on LiNbO3for a temperature stable SAW device. Journal Physics D: Applied Physics, 2003, 36, 1773-1777.	2.8	25
85	Stress induced enhanced polarization in multilayer BiFeO3/BaTiO3 structure with improved energy storage properties. AIP Advances, 2015, 5, .	1.3	25
86	Ultraviolet radiation detection by barium titanate thin films grown by sol–gel hydrothermal method. Sensors and Actuators A: Physical, 2015, 230, 175-181.	4.1	25
87	Postdeposition annealing of NiOx thin films: A transition from n-type to p-type conductivity for short wave length optoelectronic devices. Journal of Materials Research, 2013, 28, 723-732.	2.6	23
88	Laser ablated ZnO thin film for amperometric detection of urea. Journal of Applied Physics, 2013, 114, .	2.5	23
89	Waveguide coupled surface plasmon resonance based electro optic modulation in SBN thin films. Applied Surface Science, 2018, 458, 139-144.	6.1	23
90	Rapid antibiotic susceptibility testing by resazurin using thin film platinum as a bio-electrode. Journal of Microbiological Methods, 2019, 162, 69-76.	1.6	23

#	Article	IF	CITATIONS
91	Low Temperature Operated NO <sub>2</sub> Gas Sensor Based on SnO <sub>2</sub> –ZnO Nanocomposite Thin Film. Advanced Science Letters, 2014, 20, 911-916.	0.2	23
92	Study of A-site and B-site Doping on Multiferroic Properties of BFO Thin Films. Ferroelectrics, 2013, 454, 41-46.	0.6	22
93	An electrochemical DNA biosensor based on Ni doped ZnO thin film for meningitis detection. Journal of Electroanalytical Chemistry, 2017, 792, 8-14.	3.8	22
94	Temperature stable LiNbO3 surface acoustic wave device with diode sputtered amorphous TeO2 over-layer. Applied Physics Letters, 2005, 86, 223508.	3.3	21
95	N-doped ZnO thin film for development of magnetic field sensor based on surface plasmon resonance. Optics Letters, 2013, 38, 3542.	3.3	21
96	Controllable one step copper coating on carbon nanofibers for flexible cholesterol biosensor substrates. Journal of Materials Chemistry B, 2016, 4, 229-236.	5.8	21
97	A contrivance based on electrochemical integration of graphene oxide nanoparticles/nickel nanoparticles for bilirubin biosensing. Biochemical Engineering Journal, 2017, 125, 238-245.	3.6	21
98	Mesoporous metal oxide–α-Fe2O3 nanocomposites for sensing formaldehyde and ethanol at room temperature. Journal of Physics and Chemistry of Solids, 2020, 145, 109536.	4.0	21
99	Effect of manganese doping on conduction in olivine LiFePO4. Journal of Materials Science: Materials in Electronics, 2017, 28, 5192-5199.	2.2	20
100	Enhanced dielectric properties and suppressed leakage current density of PVDF composites flexible film through small loading of submicron Ba0.7Sr0.3TiO3 crystallites. Journal of Materials Science: Materials in Electronics, 2017, 28, 11806-11812.	2.2	20
101	NO <sub>2</sub> Gas Sensor Based on SnSe/SnSe <sub>2</sub> <i>p-n</i> Hetrojunction. Journal of Nanoscience and Nanotechnology, 2021, 21, 4779-4785.	0.9	20
102	Magnetic hysteresis of cerium doped bismuth ferrite thin films. Journal of Magnetism and Magnetic Materials, 2015, 378, 333-339.	2.3	19
103	Structural and dielectric properties of PLD grown BST thin films. Vacuum, 2019, 159, 69-75.	3.5	19
104	Optical waveguiding and birefringence properties of sputtered zinc oxide (ZnO) thin films on glass. Optical Materials, 2004, 27, 241-248.	3.6	18
105	Transition from diamagnetic to ferromagnetic state in laser ablated nitrogen doped ZnO thin films. AIP Advances, 2015, 5, 027117.	1.3	18
106	Reduced graphene oxide-SnO2 nanocomposite thin film based CNG/PNG sensor. Sensors and Actuators B: Chemical, 2017, 245, 590-598.	7.8	18
107	Study of optical properties of Ce and Mn doped BiFeO3 thin films using SPR technique for magnetic field sensing. Vacuum, 2018, 158, 48-51.	3.5	18
108	CdSe/V <sub>2</sub> O <sub>5</sub> core/shell quantum dots decorated reduced graphene oxide nanocomposite for high-performance electromagnetic interference shielding application. Nanotechnology, 2019, 30, 505704.	2.6	18

#	Article	IF	CITATIONS
109	Insight into electronic, magnetic and optical properties of magnetically ordered Bi2Fe4O9. Journal of Magnetism and Magnetic Materials, 2019, 475, 695-702.	2.3	18
110	Nanocatalyst (Pt, Ag and CuO) Doped SnO <sub>2</sub> Thin Film Based Sensors for Low Temperature Detection of NO <sub>2</sub> Gas. Advanced Science Letters, 2014, 20, 1374-1377.	0.2	18
111	Fast Response Ultra-violet Photodetectors Based on Sol Gel Derived Ga-doped ZnO. Procedia Engineering, 2014, 94, 44-51.	1.2	17
112	Dielectric and ferroelectric studies of KNN thin film grown by pulsed laser deposition technique. Vacuum, 2019, 160, 233-237.	3.5	17
113	Refractive index tuning of SiO2 for Long Range Surface Plasmon Resonance based biosensor. Biosensors and Bioelectronics, 2020, 168, 112508.	10.1	17
114	Deposition of stress free c-axis oriented LiNbO3 thin film grown on (002) ZnO coated Si substrate. Journal of Applied Physics, 2012, 111, 102803.	2.5	16
115	Optical properties of the c-axis oriented LiNbO3 thin film. Thin Solid Films, 2012, 520, 2142-2146.	1.8	16
116	Study of energy band discontinuity in NiZnO/ZnO heterostructure using X-ray photoelectron spectroscopy. Applied Physics Letters, 2016, 108, .	3.3	16
117	Multiferroic cantilever for power generation using dual functionality. Applied Physics Letters, 2016, 109, .	3.3	16
118	Strong electromagnetic wave absorption and microwave shielding in the Ni–Cu@MoS2/rGO composite. Journal of Materials Science: Materials in Electronics, 2019, 30, 18666-18677.	2.2	16
119	Development of polyvinylidene fluoride–graphite composites as an alternate material for electromagnetic shielding applications. Materials Research Express, 2019, 6, 075324.	1.6	16
120	Reagentless uric acid biosensor based on Ni microdiscs-loaded NiO thin film matrix. Analyst, The, 2014, 139, 4606-4612.	3.5	15
121	Study on Mn-induced Jahn–Teller distortion in BiFeO3 thin films. Journal of Materials Science, 2014, 49, 5997-6006.	3.7	15
122	A ZnO–CNT nanocomposite based electrochemical DNA biosensor for meningitis detection. RSC Advances, 2016, 6, 76214-76222.	3.6	15
123	Investigation of excess and deficiency of iron in BiFeO3. Materials Chemistry and Physics, 2018, 204, 207-215.	4.0	15
124	Weak Antilocalization and Quantum Oscillations of Surface States in Topologically Nontrivial DyPdBi(110)Half Heusler alloy. Scientific Reports, 2018, 8, 9931.	3.3	15
125	Ferroelectric PZT thin films for photovoltaic application. Materials Science in Semiconductor Processing, 2020, 105, 104723.	4.0	15
126	Hydrothermal synthesis of micro-flower like morphology aluminum-doped MoS2/rGO nanohybrids for high efficient electromagnetic wave shielding materials. Ceramics International, 2021, 47, 15648-15660.	4.8	15

#	Article	IF	CITATIONS
127	Smartphone integrated handheld Long Range Surface Plasmon Resonance based fiber-optic biosensor with tunable SiO2 sensing matrix. Biosensors and Bioelectronics, 2022, 201, 113919.	10.1	15
128	Enhanced Magnetic and Electric Properties of Nanocrystalline Ce Modified BFO Thin Films. Ferroelectrics, 2014, 470, 272-279.	0.6	14
129	Effect of ion beam irradiation on dielectric properties of BaTiO3 thin film using surface plasmon resonance. Journal of Materials Science, 2016, 51, 4055-4060.	3.7	14
130	Giant Magnetoelectric Effect in PZT Thin Film Deposited on Nickel. Energy Harvesting and Systems, 2016, 3, 181-188.	2.7	14
131	Effect of laser fluence on multiferroic BiFeO3 ferroelectric photovoltaic cells. Journal of Physics and Chemistry of Solids, 2020, 146, 109602.	4.0	14
132	Development of novel MoS2 hydrovoltaic nanogenerators for electricity generation from moving NaCl droplet. Journal of Alloys and Compounds, 2021, 884, 161058.	5.5	14
133	Tunable electronic and magnetic properties of <mml:math xmlns:mml="http://www.w3.org/1998/Math/MathML" altimg="si12.svg"&gt;<mml:mrow><mml:mn>3</mml:mn><mml:mi>d</mml:mi></mml:mrow> transition metal doped Bi2Fe4O9. lournal of Magnetism and Magnetic Materials. 2020. 509. 166893.</mml:math 	2.3	13
134	Enhanced interlayer coupling and efficient photodetection response of <i>in-situ</i> grown MoS2–WS2 van der Waals heterostructures. Journal of Applied Physics, 2021, 129, .	2.5	13
135	Al:ZnO thin film: An efficient matrix for cholesterol detection. Journal of Applied Physics, 2012, 112, 114701.	2.5	12
136	Magneto-optical properties of BiFeO3 thin films using surface plasmon resonance technique. Physica B: Condensed Matter, 2014, 448, 120-124.	2.7	12
137	Study of electrical, dielectric and EMI shielding behavior of copper metal, copper ferrite and PVDF composite. Integrated Ferroelectrics, 2018, 194, 80-87.	0.7	12
138	Multiferroic BFO/BTO multilayer structures based magnetic field sensor. Physica B: Condensed Matter, 2019, 571, 1-4.	2.7	12
139	Enhanced electron transfer properties of NiO thin film for the efficient detection of urea. Materials Science and Engineering B: Solid-State Materials for Advanced Technology, 2019, 240, 147-155.	3.5	12
140	Thiol-functionalized multiwall carbon nanotubes for electrochemical sensing of thallium. Materials Chemistry and Physics, 2021, 259, 124068.	4.0	12
141	Double Schottky metal–semiconductor–metal based GaN photodetectors with improved response using laser MBE technique. Journal of Materials Research, 2022, 37, 457-469.	2.6	12
142	Table top surface plasmon resonance measurement system for efficient urea biosensing using ZnO thin film matrix. Journal of Biomedical Optics, 2016, 21, 087006.	2.6	11
143	Effect of insertion of low leakage polar layer on leakage current and multiferroic properties of BiFeO <sub>3</sub> /BaTiO <sub>3</sub> multilayer structure. RSC Advances, 2016, 6, 59150-59154.	3.6	11
144	An impedimetric response study for the efficient detection of breast cancer specific biomarker CA 15-3 using a tin oxide thin film based immunoelectrode. Analytical Methods, 2017, 9, 6549-6559.	2.7	11

#	Article	IF	CITATIONS
145	MEMS-based microheaters integrated gas sensors. Integrated Ferroelectrics, 2018, 193, 72-87.	0.7	11
146	To study the effect of MWCNT incorporated into PVDF-Graphite composites for EMI shielding applications. Materials Today: Proceedings, 2018, 5, 15348-15353.	1.8	11
147	Effect of top metal contact on the ferroelectric photovoltaic response of BFO thin film capacitors. Vacuum, 2018, 158, 117-120.	3.5	11
148	Demonstration of wide frequency bandwidth electro-optic response in SBN thin film waveguide. Optical Materials, 2018, 85, 26-31.	3.6	11
149	Comparison of Ferroelectric Photovoltaic Performance in BFO/BTO Multilayer Thin Film Structure Fabricated Using CSD & PLD Techniques. Journal of Electronic Materials, 2021, 50, 1835-1844.	2.2	11
150	Electroluminescence study of InGaN/GaN QW based p-i-n and inverted p-i-n junction based short-wavelength LED device using laser MBE technique. Optical Materials, 2022, 126, 112149.	3.6	11
151	A Simple Paper Based Microfluidic Electrochemical Biosensor for Pointâ€ofâ€Care Cholesterol Diagnostics. Physica Status Solidi (A) Applications and Materials Science, 2017, 214, 1700468.	1.8	10
152	Development of nanostructured nickel oxide thin film matrix by rf sputtering technique for the realization of efficient bioelectrode. Vacuum, 2018, 158, 68-74.	3.5	10
153	Effect of growth and electrical properties of TiOx films on microbolometer design. Journal of Materials Science: Materials in Electronics, 2020, 31, 6671-6678.	2.2	10
154	The role of an unintentional carbon dopant in resolving the controversial conductivity aspects in BiFeO <sub>3</sub> . Physical Chemistry Chemical Physics, 2020, 22, 10010-10026.	2.8	10
155	Realization of low-power and high mobility thin film transistors based on MoS2 layers grown by PLD technique. Materials Science and Engineering B: Solid-State Materials for Advanced Technology, 2021, 266, 115047.	3.5	10
156	Efficient detection of cholesterol using ZnO thin film based matrix. Journal of Experimental Nanoscience, 2013, 8, 280-287.	2.4	9
157	Influence of stress in ZnO thin films on its biosensing application. Enzyme and Microbial Technology, 2015, 79-80, 63-69.	3.2	9
158	Influence of immobilization strategies on biosensing response characteristics: A comparative study. Enzyme and Microbial Technology, 2016, 82, 144-150.	3.2	9
159	A theoretical and experimental formalism of electronic structure of BFO:Cr thin films and modulation of their electrical properties upon visible light illumination. Journal of Applied Physics, 2018, 124, 155304.	2.5	9
160	Structural, morphological and optical properties of BiFe0.99Cr0.01O3 thin films. Vacuum, 2018, 158, 166-171.	3.5	9
161	In-situ and post deposition analysis of laser MBE deposited GaN films at varying nitrogen gas flow. Vacuum, 2019, 164, 72-76.	3.5	9
162	Investigation of cadmium-incorporated ZnO thin films for photodetector applications. Superlattices and Microstructures, 2021, 151, 106812.	3.1	9

#	Article	IF	CITATIONS
163	Temperature Dependent Optical Properties of c axis Oriented LiNbO\$_{3}\$ Thin Film Using Surface Plasmon Resonance. Journal of Lightwave Technology, 2010, 28, 3004-3011.	4.6	8
164	Efficient detection of total cholesterol using (ChEt–ChOx/ZnO/Pt/Si) bioelectrode based on ZnO matrix. Thin Solid Films, 2014, 562, 612-620.	1.8	8
165	Long range surface plasmon resonance (LRSPR) based highly sensitive refractive index sensor using Kretschmann prism coupling arrangement. AIP Conference Proceedings, 2016, , .	0.4	8
166	Surface plasmon resonance aided analysis of quantum wells for photonic device applications. Materials and Design, 2018, 150, 94-103.	7.0	8
167	Facile Synthesis of Porous CuO Nanosheets as High-performance NO <sub>2</sub> Gas Sensor. Integrated Ferroelectrics, 2018, 193, 59-65.	0.7	8
168	Influence of laser fluence in modifying energy storage property of BiFeO3 thin film capacitor. Journal of Energy Storage, 2020, 32, 101769.	8.1	8
169	Room temperature electroluminescence from Laser MBE grown Gallium nitride LEDs. Materials Science and Engineering B: Solid-State Materials for Advanced Technology, 2020, 260, 114655.	3.5	8
170	Plasmon-Assisted Crystalline Silicon Solar Cell with TiO2 as Anti-Reflective Coating. Plasmonics, 2020, 15, 1091-1101.	3.4	8
171	Phase-defined growth of In2Se3 thin films using PLD technique for high performance self-powered UV photodetector. Applied Surface Science, 2022, 595, 153505.	6.1	8
172	Structural and magnetic properties of Ni-Zn doped BaM nanocomposite via citrate precursor. AIP Conference Proceedings, 2016, , .	0.4	7
173	Effect of Zr substitution on structural, magnetic, and optical properties of Bi0.9Dy0.1Fe1â^'xZrxO3 multiferroic ceramics prepared by rapid liquid phase sintering method. Ceramics International, 2017, 43, 4904-4909.	4.8	7
174	Characterization of Lead Zirconium Titanate thin films based multifunctional energy harvesters. Thin Solid Films, 2018, 652, 39-42.	1.8	7
175	Optical study of ZnS nano spheres with varying amount of ethylenediamine for photovoltaic application. Integrated Ferroelectrics, 2018, 194, 135-144.	0.7	7
176	Surface Plasmon Resonance assisted optical analysis of Strontium Barium Niobate thin films. Applied Surface Science, 2020, 501, 144178.	6.1	7
177	Role of charge states and dopant site in governing electronic properties of Cr doped BiFeO3. Materials Chemistry and Physics, 2021, 263, 124438.	4.0	7
178	ZnO Surface Acoustic Wave Sensor for the Enhanced Detection of DMMP. Solid State Phenomena, 0, 185, 69-72.	0.3	6
179	Effect of MgO and V <sub>2</sub> O <sub>5</sub> Catalyst on the Sensing Behaviour of Tin Oxide Thin Film for SO <sub>2</sub> Gas. Conference Papers in Science, 2014, 2014, 1-4.	0.3	6
180	EMI shielding of ABS composites filled with different temperature-treated equal-quantity charcoals. RSC Advances, 2019, 9, 23718-23726.	3.6	6

#	Article	IF	CITATIONS
181	Electro-optic (EO) effect in proton-exchanged lithium niobate: towards EO modulator. Applied Physics B: Lasers and Optics, 2019, 125, 1.	2.2	6
182	High-efficiency microwave absorption and electromagnetic interference shielding of Cobalt-doped MoS2 nanosheet anchored on the surface reduced graphene oxide nanosheet. Journal of Materials Science: Materials in Electronics, 2020, 31, 19895-19909.	2.2	6
183	SPR studies on optical fiber coated with different plasmonic metals for fabrication of efficient biosensors. Materials Today: Proceedings, 2020, 33, 2180-2186.	1.8	6
184	Investigation of optical non-linearity of lead-free ferroelectric potassium sodium niobate (K0.35Na0.65NbO3) thin films via two-wave mixing phenomenon. Optics and Laser Technology, 2021, 141, 107148.	4.6	6
185	Investigation of Adulteration in Milk using Surface Plasmon Resonance. ECS Journal of Solid State Science and Technology, 2021, 10, 091004.	1.8	6
186	Ferroelectric and magnetic domain mapping of magneto-dielectric Ce doped BiFeO3 thin films. Journal of Alloys and Compounds, 2021, 882, 160698.	5.5	6
187	Fe doped ZnO thin film for mediator-less biosensing application. Journal of Applied Physics, 2012, 111, .	2.5	5
188	Dielectric Properties of SnO <sub>2</sub> Thin Film Using SPR Technique for Gas Sensing Applications. Conference Papers in Science, 2014, 2014, 1-4.	0.3	5
189	Plasmonic enhancement of optical absorption of UV radiation by Au nanoparticles dispersed on ZnO thin film. Applied Physics A: Materials Science and Processing, 2014, 116, 913-919.	2.3	5
190	Optical properties of lead- free ferroelectric potassium sodium niobate (KxNa1-xNbO3) thin films. Materials Today: Proceedings, 2019, 17, 34-40.	1.8	5
191	Synthesis of mesoporous α-Fe2O3 nanostructures via nanocasting using MCM-41 and KIT-6 as hard templates for sensing volatile organic compounds (VOCs). Journal of Porous Materials, 2020, 27, 285-294.	2.6	5
192	Synthesis and characterization of sol gel derived nontoxic CZTS thin films without sulfurization. International Journal of Applied Ceramic Technology, 2020, 17, 1194-1200.	2.1	5
193	Impact of TiO2 buffer layer on the ferroelectric photovoltaic response of CSD grown PZT thick films. Applied Physics A: Materials Science and Processing, 2021, 127, 1.	2.3	5
194	Electromagnetic interference shielding properties of hierarchical core-shell palladium-doped MoS2/CNT nanohybrid materials. Ceramics International, 2021, 47, 27586-27597.	4.8	5
195	Ferroelectric and Magnetoelectric Characteristics of the PZT Thin Films Deposited On Nickel. Advanced Science Letters, 2014, 20, 1116-1119.	0.2	5
196	Nano-Crystalline SnO <sub>2</sub> Thin Film Based Surface Acoustic Wave Sensor for Selective and Fast Detection of NO <sub>2</sub> Gas. Advanced Science Letters, 2014, 20, 1124-1128.	0.2	5
197	Improved Temperature Stability of LiNbO3Surface Acoustic Wave Devices with Sputtered SiO2Over-Layers. Ferroelectrics, 2005, 329, 57-60.	0.6	4
198	Enhanced dielectric properties of multilayered BiFeO3/BaTiO3 capacitors deposited by pulsed laser deposition. AIP Conference Proceedings, 2016, , .	0.4	4

#	Article	IF	CITATIONS
199	Low temperature operated NiO-SnO2 heterostructured SO2 gas sensor. AIP Conference Proceedings, 2016, , .	0.4	4
200	Fabry-perot modes enhanced pump-probe coupling in gold micro-disk patterned ruby thin film. Optical Materials, 2017, 72, 375-379.	3.6	4
201	Influence of 100 MeV Au+8 ion on photovoltaic response of BiFeO3/BaTiO3 multilayer structures. Materials and Design, 2017, 114, 345-354.	7.0	4
202	Development of MEMS-Based Lamb Wave Acoustic Devices. IEEE Transactions on Electron Devices, 2018, 65, 1523-1528.	3.0	4
203	Growth of KNN Thin Films for Non‣inear Optical Applications. Physica Status Solidi (A) Applications and Materials Science, 2018, 215, 1700452.	1.8	4
204	Insight into the gas phase dissociation of CF3CH2I and its reactions with H and OH by first principles. Journal of Molecular Modeling, 2018, 24, 315.	1.8	4
205	Antimicrobial properties of metallic nanoparticles: a qualitative analysis. Materials Today: Proceedings, 2019, 17, 155-160.	1.8	4
206	Fabrication of micro-cantilever and its theoretical validation for energy harvesting applications. Microsystem Technologies, 2019, 25, 4249-4256.	2.0	4
207	Ferroelectric Sr0.6Ba0.4Nb2O6 thin film based broadband waveguide coupled surface plasmon electro-optic modulator. Optics and Laser Technology, 2020, 122, 105880.	4.6	4
208	Thermo-optic Aided Tunability of Sr0.6Ba0.4Nb2O6 Thin Film-based Electro-optic Modulator Using Waveguide Coupled SPR Modes. Plasmonics, 2020, 15, 661-669.	3.4	4
209	Non-volatile resistive switching in WO3thin films. AIP Conference Proceedings, 2020, , .	0.4	4
210	Growth of highly oriented orthorhombic phase of Bi2Fe4O9 thin films by pulsed laser deposition. Materials Today: Proceedings, 2021, 47, 1646-1650.	1.8	4
211	Theoretical simulations of SAW based sensor on PVDF. Materials Today: Proceedings, 2021, 47, 1538-1541.	1.8	4
212	High figure of merit observed in SBN thin film based EO modulator employing WCSPR technique. Optics and Laser Technology, 2021, 137, 106816.	4.6	4
213	Photovoltaic Properties of BiFeO <sub>3</sub> /BaTiO <sub>3</sub> Bilayered Thin Film. Advanced Science Letters, 2014, 20, 1316-1320.	0.2	4
214	Study of intrinsic point defects in $\hat{I}^3$ -In2Se3 based on first principles calculations for the realization of an efficient UV photodetector. Journal of Alloys and Compounds, 2022, 912, 165197.	5.5	4
215	Compositional, electrical and thermal properties of nonstoichiometric titanium oxide thin films for MEMS bolometer applications. Materials Science in Semiconductor Processing, 2022, 148, 106779.	4.0	4
216	The AC Conductivity and Dielectric Constant of (006) Textured LiNbO3Films. Ferroelectrics, Letters Section, 2005, 32, 125-130.	1.0	3

#	Article	IF	CITATIONS
217	Realization of Surface Acoustic Wave (SAW) and Semiconductor Gas Sensors for Room Temperature Detection of NO2 Gas. Integrated Ferroelectrics, 2013, 148, 90-95.	0.7	3
218	BiFeO <sub>3</sub> /BaTiO <sub>3</sub> Multilayer Structures for Solar Energy Harvesting Application. Energy Harvesting and Systems, 2016, 3, 237-243.	2.7	3
219	Plasmonic assisted two wave mixing phenomenon for energy transfer in ferroelectric PZT film. Optical Materials, 2017, 66, 442-446.	3.6	3
220	Structural and dielectric properties of Cu2-xNdxO nanostructures. AIP Conference Proceedings, 2018, , .	0.4	3
221	Effect of Li doping on the electronic and magnetic properties of BiFeO <sub>3</sub> by first principles. Integrated Ferroelectrics, 2018, 193, 123-128.	0.7	3
222	Effect of Pr <sup>3+</sup> substitution on structural, dielectric, electrical and magnetic properties of BiFe <sub>0.80</sub> Ti <sub>0.20</sub> O <sub>3</sub> [Bi <sub>1-x</sub> Pr <sub>x</sub> Fe <sub>0.80</sub> Ti <sub>0.20</sub> O <sub>3</sub> (sub>1-xPr <sub>x</sub> Fe <sub>0.80</sub> Ti <sub>0.20</sub> O <sub>3</sub> , x = 0.05, 0.3 ceramics. Integrated Ferroelectrics, 2018, 193, 1-13.	10 <mark>, 0</mark> .15]	3
223	Fabrication of ZnO/Si lamb wave acoustic devices. Ferroelectrics, 2018, 535, 41-46.	0.6	3
224	Laser Molecular Beam Epitaxy (LMBE) Technique grown GaN p-n junction. Materials Today: Proceedings, 2018, 5, 15361-15365.	1.8	3
225	Influence of top metal electrode on electrical properties of pulsed laser deposited lead-free ferroelectric K0.35Na0.65NbO3 thin films. Materials Science in Semiconductor Processing, 2019, 103, 104618.	4.0	3
226	Impact of plasma dynamics on magneto optic kerr effect (MOKE) in Mn doped BFO thin films. Physica B: Condensed Matter, 2019, 571, 57-63.	2.7	3
997	xmins:mmi="http://www.w3.org/1998/Wath/WathWL" altimg= si4.gir		

#	Article	IF	CITATIONS
235	Study of ferroelectric SBN thin films for electro-optic applications. , 2016, , .		2
236	Low-temperature SnO <sub>2</sub> -based conductometric SO <sub>2</sub> gas sensor. Emerging Materials Research, 2017, 6, 3-7.	0.7	2
237	Effect of Pr substitution on structural, magnetic, and optical properties of Bi1â^'xPrxFe0.80Ti0.20O3 multiferroic ceramics. Journal of Materials Science: Materials in Electronics, 2017, 28, 1011-1014.	2.2	2
238	XPS resolved surface states analysis of ZnO and Ni doped ZnO films for quantum well applications. Ferroelectrics, 2018, 534, 199-205.	0.6	2
239	High frequency Coplanar Microwave Resonator using ferroelectric thin film for Wireless Communication Applications. Materials Today: Proceedings, 2018, 5, 15395-15398.	1.8	2
240	Structural, optical and photocatalytic properties of ZnO nanostructures. AIP Conference Proceedings, 2018, , .	0.4	2
241	Tailoring in-plane magnetocrystalline anisotropy of Fe5SiB2 with Cr-substitution. AIP Conference Proceedings, 2019, , .	0.4	2
242	Enhancement of magnetic anisotropy of Fe5PB2 with W substitution: ab-initio study. AIP Conference Proceedings, 2019, , .	0.4	2
243	Texture evolution in PLD grown ferroelectric Strontium Barium Niobate (SBN) thin films with processing parameters. Superlattices and Microstructures, 2020, 148, 106732.	3.1	2
244	Enhanced Low Temperature Thermoelectric Properties by Nano-Inclusion of 2D MoS2 with Fe:ZnO Thin Films. Journal of Electronic Materials, 2021, 50, 4567-4576.	2.2	2
245	Bipolar Resistive Switching in Magnetostrictive Ni/PZT/Pt Structure for Non-Volatile Memory Applications. ECS Journal of Solid State Science and Technology, 0, , .	1.8	2
246	BFMO/BCFO Multilayered Thin Film for Photovoltaic Application. Advanced Science Letters, 2014, 20, 971-976.	0.2	2
247	ZnO Nanostructured Thin Film as an Efficient Matrix for Total Cholesterol Detection. Advanced Science Letters, 2014, 20, 1044-1049.	0.2	2
248	Properties of Barium Titanate Thin Films Grown by Sol–Gel-Hydrothermal Process. Advanced Science Letters, 2014, 20, 1143-1146.	0.2	2
249	Structural, Optical, and Electrical Properties of Thin Films of Bismuth Tri-Iodide. Advanced Science Letters, 2014, 20, 1442-1445.	0.2	2
250	Enhanced Pyroelectric Coefficient in Ferroelectric Lead Zirconium Titanate Thick Films for Thermal Energy Harvesting Applications. ECS Journal of Solid State Science and Technology, 2022, 11, 023015.	1.8	2
251	Studies on energy storage properties of <scp>BFO</scp> / <scp>WO<sub>3</sub></scp> bilayer thin film capacitor. Energy Storage, 2023, 5, .	4.3	2
252	Optical Waveguiding Properties of RF Diode Sputtered LiNbO3Thin Films. Ferroelectrics, 2005, 329, 61-64.	0.6	1

#	Article	IF	CITATIONS
253	Reagentless detection of uric acid based on Iron doped Zinc Oxide matrix. , 2012, , .		1
254	Effect of Dispersal of Pd Nanocatalysts on H2 Sensing Response of SnO2 Thin Film Based Gas Sensor. Materials Research Society Symposia Proceedings, 2013, 1494, 327-332.	0.1	1
255	NO2 Sensing Properties of WO3 Thin Films Deposited by Rf-Magnetron Sputtering. Conference Papers in Science, 2014, 2014, 1-5.	0.3	1
256	Stabilization of Ferromagnetism in Co Codoped ZnO:N. Integrated Ferroelectrics, 2014, 158, 90-97.	0.7	1
257	Multiferroic BiFeO <sub>3</sub> /BaTiO <sub>3</sub> thin films fabricated by chemical solution deposition technique. Materials Research Society Symposia Proceedings, 2015, 1805, 1.	0.1	1
258	Dielectric dispersion of rf Sputter-deposited SnO <sub>2</sub> , ZnO, WO <sub>3</sub> thin films using surface plasmon resonance technique. IEEE Transactions on Dielectrics and Electrical Insulation, 2015, 22, 3529-3535.	2.9	1
259	WO3/BTO heterostructures based NO2sensor with enhanced response characteristics. Integrated Ferroelectrics, 2018, 193, 106-120.	0.7	1
260	Novel designs of SAW devices for highly sensitive chemical sensors. Materials Today: Proceedings, 2018, 5, 15371-15375.	1.8	1
261	Growth of ternary CdxZn1â^'xO thin films in oxygen ambient using pulsed laser deposition. AIP Conference Proceedings, 2018, , .	0.4	1
262	Study of half-metallicity in BiMnxFe1-xO3. AIP Conference Proceedings, 2018, , .	0.4	1
263	Demonstration of efficient SBN thin film based miniaturized Mach Zehnder EO modulator. Materials Chemistry and Physics, 2021, 262, 124300.	4.0	1
264	Enhancement in the Dielectric Property of Thick Lead Zirconium Titanate Films under UV Illumination. Physica Status Solidi (A) Applications and Materials Science, 2021, 218, 2000728.	1.8	1
265	Exploitation of electric field assisted optical signal amplification in ferroelectric photorefractive K0.50Na0.50NbO3 thin film. Optical Materials, 2021, 121, 111599.	3.6	1
266	Room Temperature Efficient Detection of NH <sub>3</sub> Using Surface Plasmon Resonance (SPR) Technique. Advanced Science Letters, 2014, 20, 966-970.	0.2	1
267	A Mediator-Less Urea Biosensor Based on Ni Doped ZnO Thin Film. Advanced Science Letters, 2014, 20, 1005-1011.	0.2	1
268	Analysis of the <i>l–V</i> Characteristics of the ln/ <i>p</i> -NiO/Pt/Si Schottky Diode. Advanced Science Letters, 2014, 20, 1077-1080.	0.2	1
269	Pd Loaded SnO2 Thin Film Based CH4 Gas Sensor. Advanced Science Letters, 2014, 20, 1056-1060.	0.2	1
270	Reliability and Reproducibility Study on Hand-Held Liquefied Petroleum Gas Sensors Based on Sputtered SnO <sub>2</sub> Thin Film and Micro-Heater Using Pt Catalyst. Advanced Science Letters, 2014, 20, 953-958.	0.2	1

#	Article	IF	CITATIONS
271	Probing Temperature Dependent Dielectric and Optical Properties of WO3 Thin Films by Surface Plasmon Resonance Technique. Advanced Science Letters, 2014, 20, 1522-1525.	0.2	1
272	Hydrothermally Synthesized Flower-Like Zinc Oxide Nanostructured Matrix for Amperometric Biosensors with Enhanced Response. Advanced Science Letters, 2014, 20, 1337-1346.	0.2	1
273	Electrocatalytic Properties of ZnO Thin Film Based Biosensor for Detection of Uric Acid. Springer Proceedings in Materials, 2022, , 1-16.	0.3	1
274	Optical Confinement Study of Laser MBE Grown InGaN/GaN Quantum Well Structure using Surface Plasmon Resonance Technique. Plasmonics, 0, , 1.	3.4	1
275	Role of vacancies in tuning the electronic and magnetic properties of BiCoO <sub>3</sub> . Physica Scripta, 2022, 97, 075819.	2.5	1
276	Room temperature detection of trace level NO <inf>2</inf> gas using SnO <inf>2</inf> nanoclusters. , 2011, , .		0
277	Influence of post-deposition annealing on structural, optical and electrical characteristics of NiO/ZnO thin film hetero-junction. Materials Research Society Symposia Proceedings, 2012, 1394, 68.	0.1	0
278	Surface Plasmon Resonance based optical temperature sensor using ZnO:N thin film. Materials Research Society Symposia Proceedings, 2012, 1399, 1.	0.1	0
279	An efficient uric acid biosensor based on tin oxide thin film matrix. Materials Research Society Symposia Proceedings, 2013, 1530, .	0.1	0
280	An efficient urea biosensor based on laser ablated ZnO thin film. Materials Research Society Symposia Proceedings, 2013, 1530, 1.	0.1	0
281	Thickness Dependent Optical Properties of WO3 Thin Film using Surface Plasmon Resonance. Materials Research Society Symposia Proceedings, 2013, 1494, 233-238.	0.1	0
282	Prominent photovoltaic response in multiferroic BFO/BTO heterostructures. , 2016, , .		0
283	Development of metal oxide thin films for self power generating integrated devices. , 2016, , .		0
284	SAW field and acousto-optical interaction in ZnO/AlN/sapphire structure. , 2016, , .		0
285	Coplanar waveguide resonator using PLZT thin film. Ferroelectrics, 2017, 515, 8-12.	0.6	0
286	Study of birefringence and electro-optic effect in SBN60 thin film. Ferroelectrics, 2018, 533, 35-42.	0.6	0
287	Emergence of magnetism in silicene by introducing carbon atom as foreign atom in all possible ways. Integrated Ferroelectrics, 2018, 194, 53-59.	0.7	0
288	Observation of high magnetocrystalline anisotropy on Co doping in rare earth free Fe2P magnetic material. AIP Conference Proceedings, 2018, , .	0.4	0

#	Article	IF	CITATIONS
289	Dynamically tuneable PLD grown SBN75 thin film based Electro optic modulator. MRS Advances, 2019, 4, 2265-2269.	0.9	0
290	Investigation on Physical Properties of Sn-Modified Cubic Cu2O Nanostructures. Journal of Superconductivity and Novel Magnetism, 2019, 32, 1671-1679.	1.8	0
291	Role of H impurity as compensating center in BiFeO <sub>3</sub> by first-principle calculations. Physica Scripta, 2021, 96, 125813.	2.5	0
292	Influence of Doping of Different Metals on the Photoconducting Properties of ZnO Thin Films. Advanced Science Letters, 2014, 20, 994-1000.	0.2	0
293	Specific Detection of Breast Cancer by Means of Electrochemical Biosensor. Advanced Science Letters, 2014, 20, 1072-1076.	0.2	0
294	Role of Au Incorporated on the Surface of ZnO Thin Film in Enhancing the UV Photoresponse. Advanced Science Letters, 2014, 20, 1437-1441.	0.2	0
295	Effect of Vacancies on Structural and Magnetic Properties of BiFeO3. Advanced Science, Engineering and Medicine, 2018, 10, 741-744.	0.3	0
296	To Study the Zinc Metal Powder Filled Polyvinylidene Fluoride Composite for Electromagnetic Interference Shielding Applications. Advanced Science, Engineering and Medicine, 2018, 10, 764-766.	0.3	0
297	Microwave absorption and reflection behaviour of polypyrrole-PMMA-Co0.5Ni0.5Fe2O4 nanocomposite in x-band. AlP Conference Proceedings, 2020, , .	0.4	0
298	Lattice-strain engineered KxNa1-xNbO3 thin films near the morphotropic phase boundary for enhanced electrical properties. Materials Chemistry and Physics, 2022, 277, 125512.	4.0	0
299	Effect of different anode electrodes with Li(Li0.25Co0.37Mn0.38)O2 as cathode material on Li: ion battery performance. Journal of Materials Science: Materials in Electronics, 2022, 33, 3901-3913.	2.2	0
300	Low-Cost and Disposable Electrochemical Paper-Based Analytical Device (PAD) for <i>Escherichia coli</i> O157:H7. Analytical Letters, 0, , 1-11.	1.8	0
301	Optical properties of LMBE grown c-axis oriented GaN thin films using Surface Plasmon Resonance technique. Optical Materials, 2022, 131, 112603.	3.6	0